# Application of incomplete similarity theory for estimating maximum shear layer thickness of granular flows in rotating drums

**Nian-Sheng Cheng [*], Qi Zhou [1], Soon Keat Tan**

*School of Civil and Environmental Engineering, Nanyang Technological University, Nanyang Avenue, Singapore 639798*

**Abstract** Granular flow in a rotating drum provides a convenient system for investigating mixing, segregation and general properties of granular materials. This study is concerned with the maximum thickness of the flowing surface layer observed at the rolling regime. A scaling relation is first derived with the consideration of incomplete similarity associated with the drum-particle size ratio and the Froude number. Calibration is then carried out with published laboratory data, which were collected for the case of rotating drums half-filled with glass beads. The scaling relation is also compared with other kinds of datasets, showing good agreement and possibilities of the proposed approach to be further extended to more complex cases.

***Keywords:*** granular flow; rotating drum; shear layer; scaling; incomplete similarity

[*] Corresponding author. School of CEE, Blk N1, Nanyang Avenue, Singapore 639798. Tel: 65- 6790 6936; Fax: 65-6791 0676; Email: cnscheng@ntu.edu.sg

[1] Present address: Environmental Fluid Mechanics Laboratory, Stanford University, Stanford, CA 94305, USA.

## 1. Introduction

Rotating drums are not only engineering devices for the purpose of mixing, drying or coating of granular materials, but also provide convenient systems for the investigation of the mechanics of granular flows. Different flowing regimes may occur depending on the rotational speed of the drum. At the rolling regime, which is considered in this study, the upper surface of the flowing layer is nearly flat and the flow is continuous and steady. The rolling regime usually occurs when the rotational speed is moderately slow. Two distinct flow regions of granular particles can be identified, one large portion undergoing solid-body rotation together with the drum and the lens-shaped surface layer flowing downwards the slope, as illustrated in Fig. 1. The surface layer is thin but characterized by high shear, and thus plays a significant role in mass and heat transfer in the granular system. Many studies have been done previously in this respect. For example, experiments have been conducted to investigate the slope of the shear-layer surface or dynamic angle of repose [1], the cross-sectional shape of the layer and the shear thickness [1-3], the profile of the surface velocity [3-5], and the velocity distribution through the flowing layer [2, 5-9]. In comparison, theoretical effort addressing the flowing layer is still challenging in the choice of the stress constitutive equation [8].

This paper is limited to the investigation of the maximum thickness of the shear layer, which serves as one of simple quantities in the description of the flowing surface layer. Several experimental studies of the maximum thickness are available in the literature. One of the important contributions is due to Felix et al. [9, 10], who conducted extensive measurements of the flowing zone thickness using rotating drums half-filled with glass beads. In their studies, the maximum thickness of the flowing zone was measured based

on CCD camera images. The bead diameter $d$, drum diameter $2R$ and drum width $W$ varied from 0.075 to 2 mm, 5.6 to 50 cm and 0.6 to 6 cm, respectively. The authors reported that the distances between the end-walls did not have significant effect on the flowing zone thickness. The angular speed of rotation $\omega$ varied from 0.209 to 2.618 rad/s to ensure that the flow was at the rolling regime. As a result, the drum-particle size ratio $R/d$ varied from 23.5 to 3700 and the Froude number $\omega^2 R/g$ varied from $5.0\times10^{-5}$ to $6.7\times10^{-2}$. Other similar measurements have also been reported in the literature for a range of particle properties, i.e. material, shape, and size, as well as drum operational parameters, i.e. size, rotational speed and fill fraction [5, 11-13].

In addition to the experimental observations, analytical efforts in developing scaling relations for the maximum thickness of the shear layer were also reported. Using different sets of dimensionless variables, Weir et al. [14] proposed two regression models:

$$\frac{\delta}{d} = n_1 \lambda_1 \left(\frac{d}{R}\right)^{n_2} Fr^{n_3} F^{n_4} \tag{1}$$

and

$$\frac{\delta}{L} = n_5 \lambda_2 \left(\frac{d}{L}\right)^{n_6} Fr^{n_7} \tag{2}$$

where $\delta$ is the maximum shear layer thickness, $F$ is the fill fraction, $L$ is the half length of the shear layer, $n_1$-$n_7$ are constants, and $\lambda_1$ and $\lambda_2$ are author-dependent parameters. In Weir et al.'s study, significant deviations were found associated systematically with different data sources and then taken into account using $\lambda_1$ and $\lambda_2$. Their data fitting results show that the variation of $\lambda_1$ and $\lambda_2$ is not small, ranging from 0.2-1.6 and 0.1-1.3, respectively. Liu et al. [15] expressed the maximum thickness as a complex function of

the dynamic angle of repose, the fill angle and the Froude number, and the related predictions exhibit large deviations from measurements.

The objective of this study is to adopt a different approach to formulate the scaling relations for the maximum thickness. The mathematical tool developed here is based on the incomplete similarity theory, which has been proved successful in several fields, for example, turbulent pipe flows [16] and open channel hydraulics [17]. The scaling relations are then derived with the relevant coefficients being evaluated with published laboratory data.

## 2. Dimensional analysis

First, dimensional analysis is carried out. The target parameter is the maximum thickness of the layer which appears around the middle of the sloping surface (Fig. 1). To simplify the derivation of the scaling relation, we first consider the case with the following limitations:

(a) The axis of the drum is horizontal. The drum is circular in shape and its width is sufficiently large so that the end-wall effects need not be considered.

(b) The particles are spherical in shape, non-cohesive, and homogeneous in size.

(c) The drum is half-filled with the particles.

(d) The particle flow occurs at the rolling regime. The flow is continuous and the flowing surface is flat.

(e) The effect of the interstitial fluid is ignored and thus the density and viscosity of the fluid are not considered.

With these simplifications, the maximum thickness for half-filled drum, $\delta_{50}$, would depend on the four parameters shown as follows:

$$\delta_{50} = \mathrm{f}\,(d, R, \omega, g) \tag{3}$$

where $d$ is the particle diameter, $R$ is the drum radius, $\omega$ is the angular speed of rotation, and $g$ is the gravitational acceleration. In dimensionless form, Eq. (3) can be rewritten as

$$\frac{\delta_{50}}{d} = \Phi\left(\frac{R}{d}, \frac{\omega^2 R}{g}\right) = \Phi(s, Fr) \tag{4}$$

In Eq. (4), the selected independent dimensionless parameters are the drum-particle size ratio $R/d$, denoted as $s$, and the Froude number $\omega^2 R/g$, denoted as $Fr$. The dependence implied by Eq. (4) is actually consistent with the laboratory observations reported by Orpe and Khakhar [1] and Felix et al. [9, 10]. Examples of the dependence are presented in Fig. 2 and Fig. 3. In Fig. 2, the variations of $\delta_{50}/d$ with $Fr$ for given $s$ are plotted. It shows a power-law dependence of $\delta_{50}/d$ on $Fr$ when $s$ is constant, i.e.

$$\frac{\delta_{50}}{d} = a_1 Fr^{a_2} \tag{5}$$

where $a_1$ and $a_2$ are constants. It is also noted that the values of $a_1$ and $a_2$ vary and are dependent on $s$. Similar to Fig. 2, Fig. 3 reveals a power-law dependence of $\delta_{50}/d$ on $s$ when $Fr$ is constant,

$$\frac{\delta_{50}}{d} = a_3 s^{a_4} \tag{6}$$

where $a_3$ and $a_4$ are also constants for given $Fr$. To construct the proper mathematical form incorporating the power-law dependences shown in both Eqs. (5) and (6), one could naturally take a simple multiplication of the power-law terms

$$\frac{\delta_{50}}{d} = b_1 Fr^{b_2} s^{b_3}, \tag{7}$$

where $b_1$, $b_2$ and $b_3$ are constants. Applying the least-squares fitting with Felix et al.'s data [9, 10] yields

$$\frac{\delta_{50}}{d} = 1.89 Fr^{0.168} s^{0.665} \tag{8}$$

The multiplicative power function given by Eq. (7) or (8) is able to provide an approximate representation of the experiment data. However, it could be significantly improved by applying the incomplete similarity theory.

In the following, the incomplete similarity theory is adopted to deduce an alternative relation incorporating both dependences on *s* and *Fr*. This theory was developed by Barenblatt [18]. Consider the following function,

$$\Pi = \Phi(\Pi_1, \Pi_2) \tag{9}$$

where $\Pi$, $\Pi_1$ and $\Pi_2$ are dimensionless parameters. For sufficiently large or small $\Pi_1$ and constant $\Pi_2$, the complete similarity exists in $\Pi_1$ if $\Phi$ has a non-zero limit, and otherwise, the incomplete similarity holds in $\Pi_1$ if $\Phi$ approaches zero or infinite. The application of the complete similarity appears limited for many problems. For the incomplete similarity, the following power-law asymptotic may apply for sufficient large or small $\Pi_1$:

$$\Pi = C\Pi_1^{\alpha} \tag{10}$$

where C and $\alpha$ are generally dependent on $\Pi_2$ [18].

Now we examine the relationship given by Eq. (4), i.e. $\delta_{50}/d = \Phi(s, Fr)$. From the observation by Felix et al. [9], it follows that $\delta_{50}/d$ would approach infinity when *s* is sufficiently large, and approach zero as *Fr* or the rotational speed is sufficiently small. It should be mentioned that with the incomplete similarity theory, it is the asymptotic,

rather than the limit, that is considered in the derivation. For this study, the concern is physically restricted to the rolling regime. If the rotating speed is extremely small, the flow would actually become intermittent, in the form of avalanche. Therefore, for the case of very small *Fr*, $\delta_{50}/d$ is considered small only in the sense of time-average.

With the above consideration, it is assumed that the incomplete similarity exists in both *s* and *Fr*, and thus the following two power-law relations apply:

$$\frac{\delta_{50}}{d} = f_1(Fr)s^{f_2(Fr)} \tag{11}$$

$$\frac{\delta_{50}}{d} = g_1(s)Fr^{g_2(s)} \tag{12}$$

where $f_1$ and $f_2$ depend on *Fr* only; and $g_1$ and $g_2$ depend on *s* only. Taking logarithms of Eqs. (11) and (12) and differentiating with respect to *Fr* gives

$$\frac{\partial[\ln(\frac{\delta_{50}}{d})]}{\partial Fr} = \frac{1}{f_1}\frac{df_1}{dFr} + \frac{df_2}{dFr}\ln(s) \tag{13}$$

$$\frac{\partial[\ln(\frac{\delta_{50}}{d})]}{\partial Fr} = g_2\frac{1}{Fr} \tag{14}$$

By assuming that the above two partial derivatives are identical, we get

$$g_2 = \frac{Fr}{f_1}\frac{df_1}{dFr} + Fr\frac{df_2}{dFr}\ln(s) \tag{15}$$

Furthermore, by noting that $g_2$ is a function of *s* only, and $f_1$ and $f_2$ are related to *Fr* only, the items involving *Fr* in Eq. (15) should be taken to be constant. Hence,

$$\frac{Fr}{f_1}\frac{df_1}{dFr} = const \tag{16}$$

$$Fr\frac{df_2}{dFr} = const \tag{17}$$

Integration of Eqs. (16) and (17) yields

$$f_1 = c_1 Fr^{c_2} \tag{18}$$

$$f_2 = c_3 \ln(Fr) + c_4 \tag{19}$$

where $c_1$, $c_2$, $c_3$ and $c_4$ are constants. Therefore, with Eqs. (11), (18) and (19), the scaling relation for the maximum shear layer thickness, based on the incomplete similarity argument with respect to the drum-particle size ratio $s$, could be written in the form of

$$\frac{\delta_{50}}{d} = c_1 Fr^{c_2} s^{c_3 \ln(Fr)+c_4} \tag{20}$$

Similarly, applying the incomplete similarity in $Fr$ yields

$$g_1 = c_5 s^{c_6} \tag{21}$$

$$g_2 = c_7 \ln(s) + c_8 \tag{22}$$

and thus,

$$\frac{\delta_{50}}{d} = c_5 s^{c_6} Fr^{c_7 \ln(s)+c_8} \tag{23}$$

where $c_5$, $c_6$, $c_7$ and $c_8$ are constants. Mathematically, it can be shown that $c_5$, $c_6$, $c_7$ and $c_8$ are equal to $c_1$, $c_4$, $c_3$ and $c_2$, respectively. By taking logarithms of both sides of Eqs. (20) and (23), one gets

$$\begin{aligned} \ln(\frac{\delta_{50}}{d}) &= \ln(c_1) + c_2 \ln(Fr) + c_3 \ln(Fr)\ln(s) + c_4 \ln(s) \\ &= \ln(c_5) + c_8 \ln(Fr) + c_7 \ln(Fr)\ln(s) + c_6 \ln(s) \end{aligned} \tag{24}$$

Eq. (24) holds irrespective of the values of $Fr$ and $s$, thus

$$c_1 = c_5,\ c_2 = c_8,\ c_3 = c_7,\ c_4 = c_6. \tag{25}$$

With the functional forms derived above, it is now possible to calibrate the empirical coefficients with the laboratory data of Felix et al. [9, 10]. Table 1 summarizes the data ranges covered in Felix et al. [9, 10] and other experimental studies. To evaluate the coefficients, Eq. (20) or Eq. (23) are expressed in the corresponding logarithmic form, i.e. Eq. (24), and then the least-squares fitting method is applied with Felix et al.'s data [9, 10]. With the empirical constants obtained, Eq. (20) and Eq. (23) are rewritten as

$$\frac{\delta_{50}}{d} = 0.389 Fr^{-0.109} s^{0.0551\ln(Fr)+0.976} = 0.389 s^{0.976} Fr^{0.0551\ln(s)-0.109} \tag{26}$$

Eq. (26) is different from the regular power law correlation, Eq. (8), in that the exponents associated with the variables, *Fr* and *s*, are generally not constant.

The predictions by the multiplicative power law, i.e. Eq. (8), and those using Eq. (26) are compared in Fig. 4 (a) and (b). Three statistical parameters are used to assess the goodness of the proposed correlation, i.e. average relative error given by $err_1 = \frac{1}{n}\sum\left[\left|(\delta_{50}/d)_{\text{cal}} - (\delta_{50}/d)_{\text{exp}}\right| / (\delta_{50}/d)_{\text{exp}}\right] \times 100\%$, where *n* is the total number of data points used; sum of squared errors defined by $err_2 = \sum\left[(\delta_{50}/d)_{\text{cal}} - (\delta_{50}/d)_{\text{exp}}\right]^2 / (\delta_{50}/d)_{\text{exp}}{}^2$; and sum of deviation defined using the logarithmic dimensionless thickness, $err_3 = \sum\left[\log(\delta_{50}/d)_{\text{cal}} - \log(\delta_{50}/d)_{\text{exp}}\right]^2$ . The values of the three parameters associated with the predictions of Eqs. (8) and (26) are shown in Table 2. It can be seen that the correlations based on incomplete similarity theory give a much better presentation of the experimental data, as compared to the simple power law. For example, $err_1$ reduces from 10.6% to 7.4% and $err_2$ reduces from 6.6 to 3.7, by applying the incomplete similarity technique.

## 3. Comparison with other studies

In Eq. (3), only four independent variables are used for the dimensional analysis. In this section, effects of two more factors, drum width and fill fraction, are considered. We will examine how the proposed model may deviate and in what way it can be generalized for more universal applications.

### *3.1. Effect of drum width*

First, consider quasi-two-dimensional rotating drums, such as those presented by Orpe and Khakhar [1] and Jain et al. [7]. Orpe and Khakhar reported the layer thickness profiles for steel balls, glass beads and sand of various sizes at dry condition using flow visualization [1]. Jain et al. measured the layer thickness for steel beads submerged in various interstitial fluids including air, water and glycerin-water mixture, using particle tracking velocimetry (PTV) [7]. Figs. 6 and 7 show that the predictions based on Eq. (26) generally agree with the two sets of data. For Orpe and Khakhar's data [1], the average relative error of the predictions is 15.6%; and for Jain et al. [7], the error is 10.5%.

However, for both cases, the prediction on average is larger than the measurement. This can be explained by noting that the particle flow is affected by both end-walls for the case of the two-dimensional rotating drum. Table 1 shows that for Felix et al.'s data [9, 10], the ratio of drum width to particle diameter, $W/d$, ranges from 5-140. These values are relatively high, indicating the prevailing three-dimensional flows in their systems. In comparison, the studies by Orpe and Khakhar [1] and Jain et al. [7] could be classified as quasi-two-dimensional in which $W/d$ varied in a narrow range, i.e. 2.5-5 and 3.2-3.4, respectively. Therefore, the general overestimation based on Eq. (26) (see Fig. 5 and Fig. 6) could be associated with the significant wall-particle interaction inherent in

the quasi-two-dimensional systems. In addition, Figs. 6 and 7 appear to indicate that the material of the particles and the interstitial fluids could have insignificant effects on the maximum shear layer thickness.

### *3.2. Effect of fill fraction*

The discussion is now extended to the effect of fill fractions other than 50%. The dimensional analysis above is limited to the cases that the drum is half filled. To include the effect of the fill fraction in this study, the functional relation in Eq. (3) is first modified by including an additional parameter representing the fill fraction. Here, we choose the depth of the granular matter measured perpendicular to the flowing surface at the mid-position or the maximum granular layer depth, $H$, which could be easily calculated based on the fill fraction and drum size. Hence, the maximum shear layer thickness for any fill fraction, $\delta$, is expressed as follows,

$$\delta = \mathrm{f}\,(d, R, H, \omega, g) \tag{27}$$

In dimensionless form, we further assume that

$$\frac{\delta}{d} = \Phi\left(\frac{\delta_{50}}{d}, \frac{H}{d}\right) \tag{28}$$

where $\delta_{50}/d$ is the dimensionless maximum shear layer thickness for half-filled drum. By noting that when either $\delta_{50}/d$ or $H/d$ is sufficiently small, $\delta/d$ approaches zero, one could assume the incomplete similarity exists both in $\delta_{50}/d$ and $H/d$. As a result, Eq. (28) could be rewritten, by following the previous analysis, as

$$\frac{\delta}{d} = c_9\left(\frac{H}{d}\right)^{c_{10}}\left(\frac{\delta_{50}}{d}\right)^{c_{11}\ln\left(\frac{H}{d}\right)+c_{12}} \tag{29}$$

where $c_9$, $c_{10}$, $c_{11}$ and $c_{12}$ are constants. By taking logarithms of both sides of Eq. (29) and applying Eq. (24), with appropriate manipulation, we get

$$\ln(\frac{\delta}{d}) = c_1' + c_2' \ln(Fr) + c_3' \ln(s) + c_4' \ln(\frac{H}{d}) + c_5' \ln(Fr)\ln(s) + c_6' \ln(\frac{H}{d})\ln(Fr) + c_7' \ln(\frac{H}{d})\ln(s) + c_8' \ln(\frac{H}{d})\ln(Fr)\ln(s) \quad (30)$$

where $c_1'$ - $c_8'$ are constants. Calibrating of the coefficients in Eq. (30) with the data summarized by Weir et al. [14], except for those by Felix et al. [10], yields

$$\frac{\delta}{d} = 5.56 \times 10^{-7} Fr^{m_1} s^{m_2} (\frac{H}{d})^{2.64} \quad (31)$$

where $m_1 = -1.73 + 0.505\ln(s) + 0.218\ln(H/d) - 0.0617\ln(H/d)\ln(s)$ and $m_2 = 3.45 - 0.465\ln(H/d)$. As shown in Fig. 7, Eq. (31) is able to give a better correlation among the four dimensionless variables, in comparison with the regression models proposed by Weir et al. [14], the latter requiring the selection of the author-dependent coefficient. The average relative error of the prediction is 17.1%. It can be expected that such functions derived with the incomplete similarity consideration may be further extended to include more factors.

## 4. Conclusions

The expression for estimating the maximum thickness of shear layer observed in a rotating drum is derived by considering the incomplete similarity with respect to the Froude number and drum-particle size ratio. The empirical coefficients are evaluated using laboratory data for the case of 50% filled drums. The proposed model also provides reasonable predictions for the case of two-dimensional drums. This study finally shows that the effect of the fill fraction or other factors can also be considered with the incomplete similarity argument.

## Acknowledgement

The support from DHI-NTU Centre and Maritime Research Centre, Nanyang Technological University, Singapore for this study is gratefully acknowledged.

## References

[1] Orpe AV, Khakhar DV. Scaling relations for granular flow in quasi-two-dimensional rotating cylinders. Physical Review E. 2001 Sep;64(3).
[2] Bonamy D, Daviaud F, Laurent L. Experimental study of granular surface flows via a fast camera: A continuous description. Physics of Fluids. 2002 May;14(5):1666-73.
[3] Ding YL, Seville JPK, Forster R, Parker DJ. Solids motion in rolling mode rotating drums operated at low to medium rotational speeds. Chemical Engineering Science. 2001 Mar;56(5):1769-80.
[4] Alexander A, Shinbrot T, Muzzio FJ. Scaling surface velocities in rotating cylinders as a function of vessel radius, rotation rate, and particle size. Powder Technology. 2002 Jul;126(2):174-90.
[5] Boateng AA, Barr PV. Granular flow behaviour in the transverse plane of a partially filled rotating cylinder. Journal of Fluid Mechanics. 1997 Jan;330:233-49.
[6] Jain N, Ottino JM, Lueptow RM. An experimental study of the flowing granular layer in a rotating tumbler. Physics of Fluids. 2002 Feb;14(2):572-82.
[7] Jain N, Ottino JM, Lueptow RM. Effect of interstitial fluid on a granular flowing layer. Journal of Fluid Mechanics. 2004 Jun;508:23-44.
[8] Orpe AV, Khakhar DV. Rheology of surface granular flows. Journal of Fluid Mechanics. 2007 Jan;571:1-32.
[9] Felix G, Falk V, D'Ortona U. Granular flows in a rotating drum: the scaling law between velocity and thickness of the flow. European Physical Journal E. 2007 Jan;22(1):25-31.
[10] Felix G, Falk V, D'Ortona U. Segregation of dry granular material in rotating drum: experimental study of the flowing zone thickness. Powder Technology. 2002 Dec;128(2-3):314-9.
[11] Henein H, Brimacombe JK, Watkinson AP. Experimental study of transverse bed motion in rotary kilns. Metallurgical Transactions B-Process Metallurgy. 1983;14(2):191-205.
[12] Van Puyvelde DR, Young BR, Wilson MA, Schmidt SJ. Modelling transverse segregation of particulate solids in a rolling drum. Chemical Engineering Research & Design. 2000 May;78(A4):643-50.
[13] Woodle GR, Munro JM. Particle motion and mixing in a rotary kiln. Powder Technology. 1993 Sep;76(3):241-5.
[14] Weir G, Krouse D, McGavin P. The maximum thickness of upper shear layers of granular materials in rotating cylinders. Chemical Engineering Science. 2005 Apr;60(7):2027-35.
[15] Liu XY, Specht E, Gonzalez OG, Walzel P. Analytical solution for the rolling-mode granular motion in rotary kilns. Chemical Engineering and Processing. 2006 Jun;45(6):515-21.
[16] Barenblatt GI, Chorin AJ, Prostokishin VM. Scaling laws for fully developed turbulent flow in pipes: Discussion of experimental data. Proceedings of the National Academy of Sciences of the United States of America. 1997 Feb;94(3):773-6.
[17] Ferro V. Simultaneous flow over and under a gate. Journal of Irrigation and Drainage Engineering-Asce. 2000 May-Jun;126(3):190-3.
[18] Barenblatt GI. Dimensional analysis: Gordon and Breach Science Publishers. 1987.

**Table 1**
Summary of experimental studies [1, 5, 7, 9-13]

| Authors | Ratio of drum radius to particle diameter, $R/d$ | Ratio of maximum granular layer depth to particle diameter, $H/d$ | Ratio of drum width to particle diameter, $W/d$ | Froude number, $Fr$ | Ratio of maximum shear layer thickness to particle diameter, $\delta/d$ or $\delta_{50}/d$ |
|---|---|---|---|---|---|
| Felix et al. [9, 10] | 23.5-3700 | 23.5-3700 | 5-140 | $4.7\times10^{-5}$-0.067 | 3.5-205 |
| Orpe and Khakhar [1] | 20-200 | 20-200 | 2.5-5 | 0.002-0.064 | 3.8-47 |
| Jain et al. [7] | 47-117 | 47-117 | 3.2-3.4 | $3.9\times10^{-5}$-$4.0\times10^{-4}$ | 4.9-12.1 |
| Boateng and Barr [5] | 90-133 | 19.5-55 | $1.9\times10^{5}$-$2.8\times10^{5}$ | $4.4\times10^{-4}$-0.015 | 6-15.7 |
| Henein et al. [11] | 46.5-400 | 8.6-180 | >95 | $8.9\times10^{-4}$ | 2.3-15 |
| Van Puyvelde et al. [12] | 40-356 | 25-94 | 20-62.5 | 0.0013-0.12 | 10.6-75.9 |
| Woodle and Munro [13] | 18.9-23.6 | 2.6-19 | - | 0.025 | 0.5-2.3 |

**Table 2**
Comparison of prediction errors

| Eq. | Prediction error | | |
|---|---|---|---|
| | Average relative error, $err_1$ (%) | Sum of squared relative errors, $err_2$ | Sum of logarithmic deviations, $err_3$ |
| (8) | 10.61 | 6.571 | 1.153 |
| (26) | 7.38 | 3.658 | 0.599 |

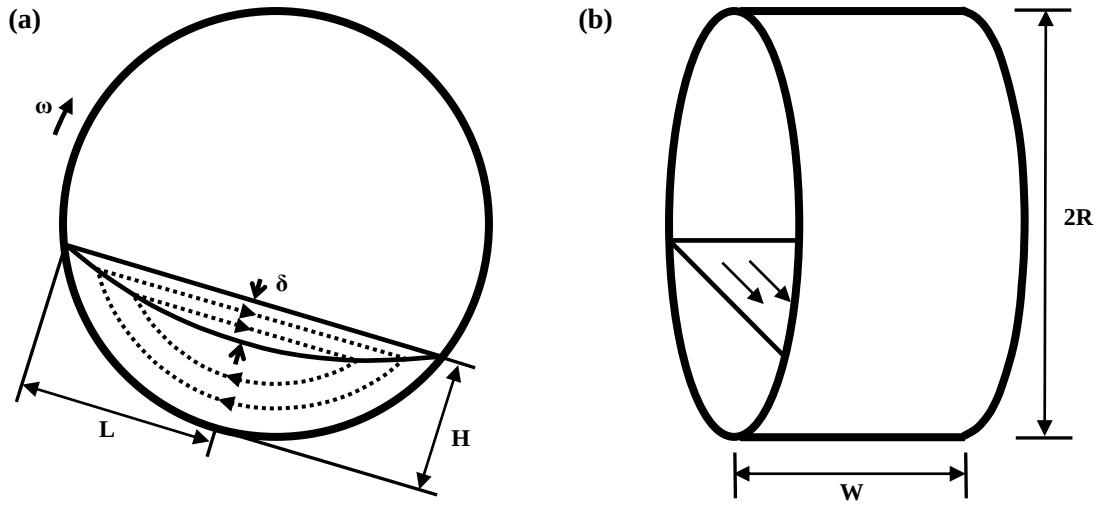


**Fig. 1.** Schematics of drum dimensions and the shear layer thickness, (a) in front view, where dotted curves indicate typical particle paths, and (b) in side view.

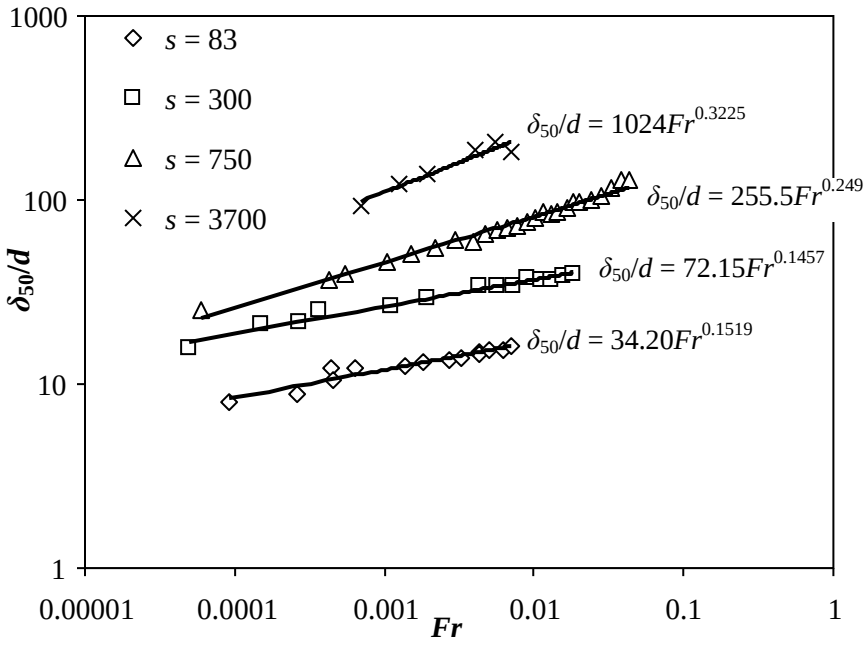


**Fig. 2.** Dimensionless maximum shear layer thickness $\delta_{50}/d$ versus Froude number $Fr$ at various drum-particle size ratios $s$ (data from Felix et al. [9, 10])**.**

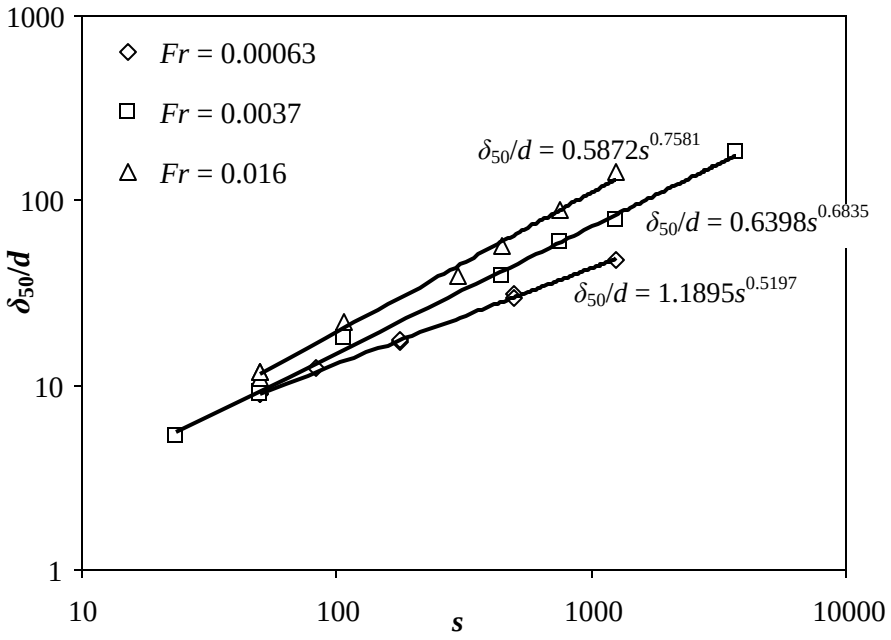


**Fig. 3.** Dimensionless maximum shear layer thickness $\delta_{50}/d$ versus drum-particle size ratio $s$ at various Froude number $Fr$ (data from Felix et al. [9, 10]).

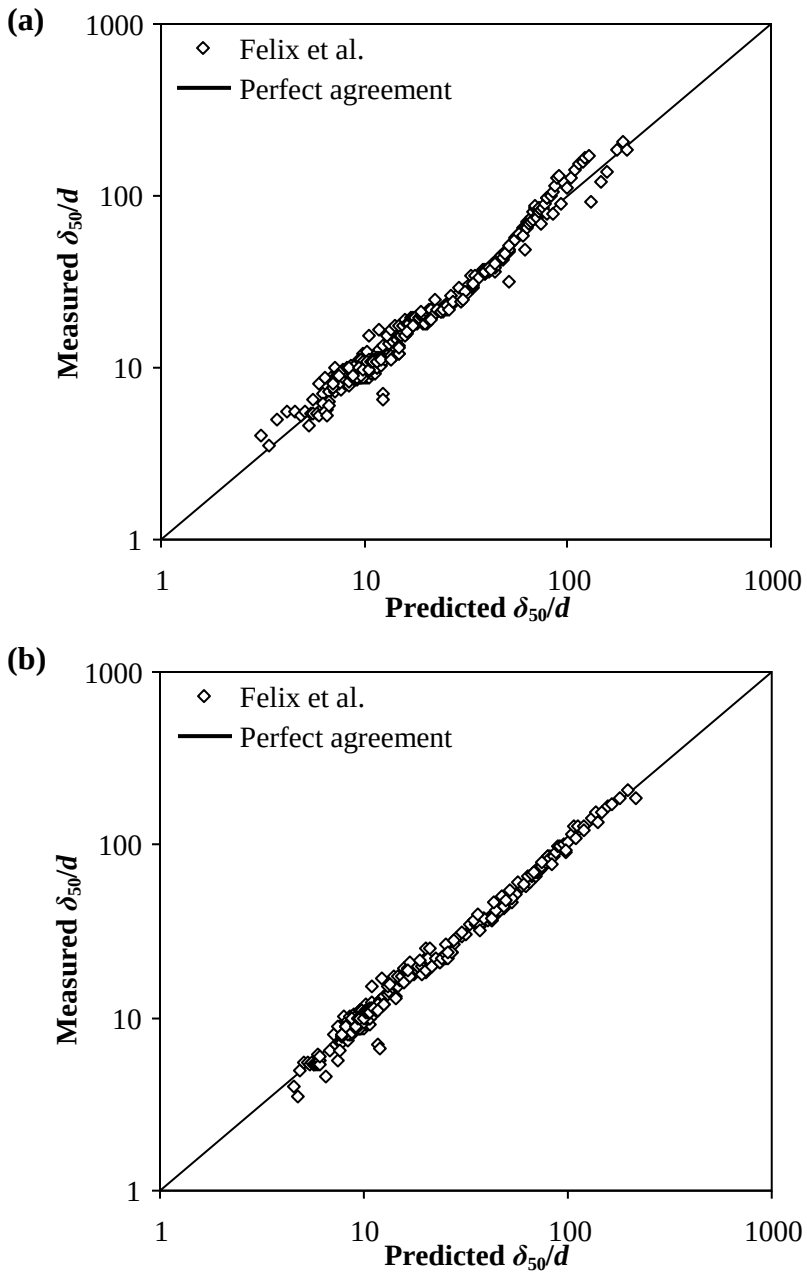


**Fig. 4.** Measured (Felix et al. [9, 10]) and predicted dimensionless maximum shear layer thickness using (a) Eq. (8) and (b) Eq. (26).

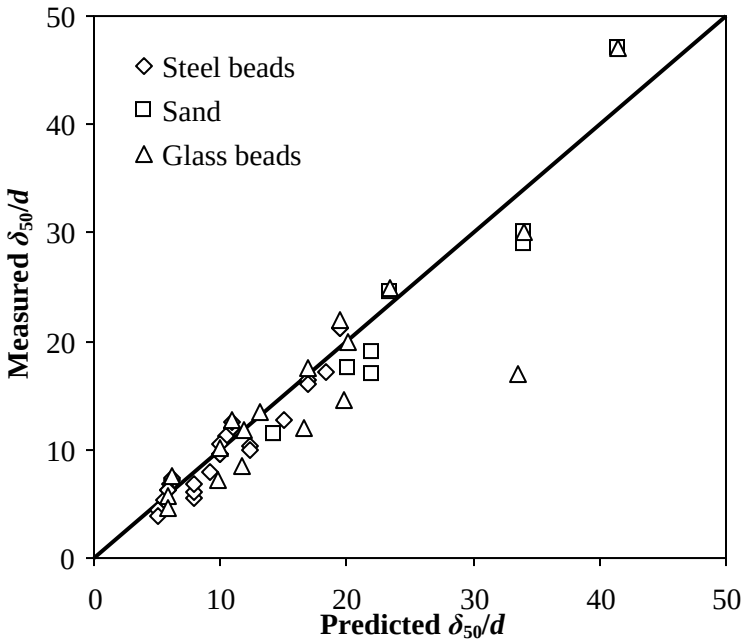


**Fig. 5.** Measured (Orpe and Khakhar [1]) and predicted dimensionless maximum shear layer thickness. Symbols indicate particle materials used. Solid line indicates perfect agreement.

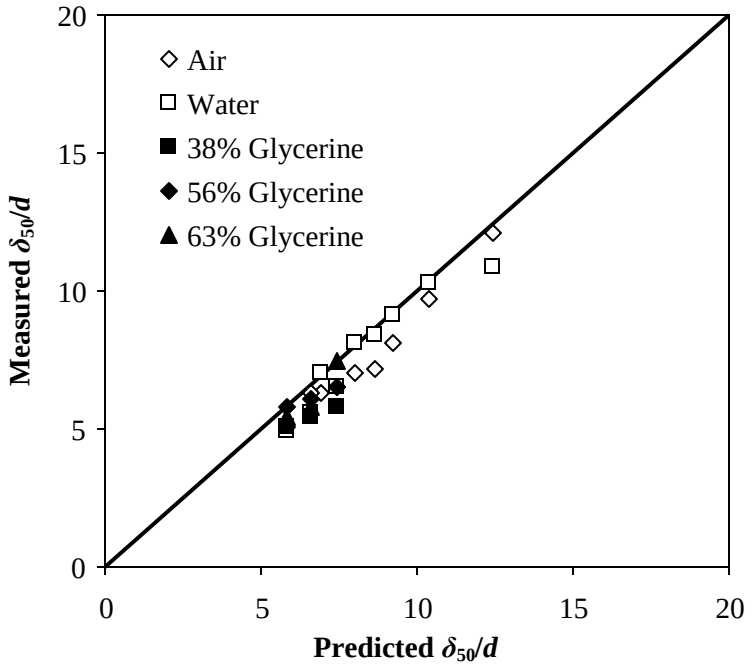


**Fig. 6.** Measured (Jain et al. [7]) and predicted dimensionless maximum shear layer thickness. Symbols indicate interstitial fluids used. Solid line indicates perfect agreement.

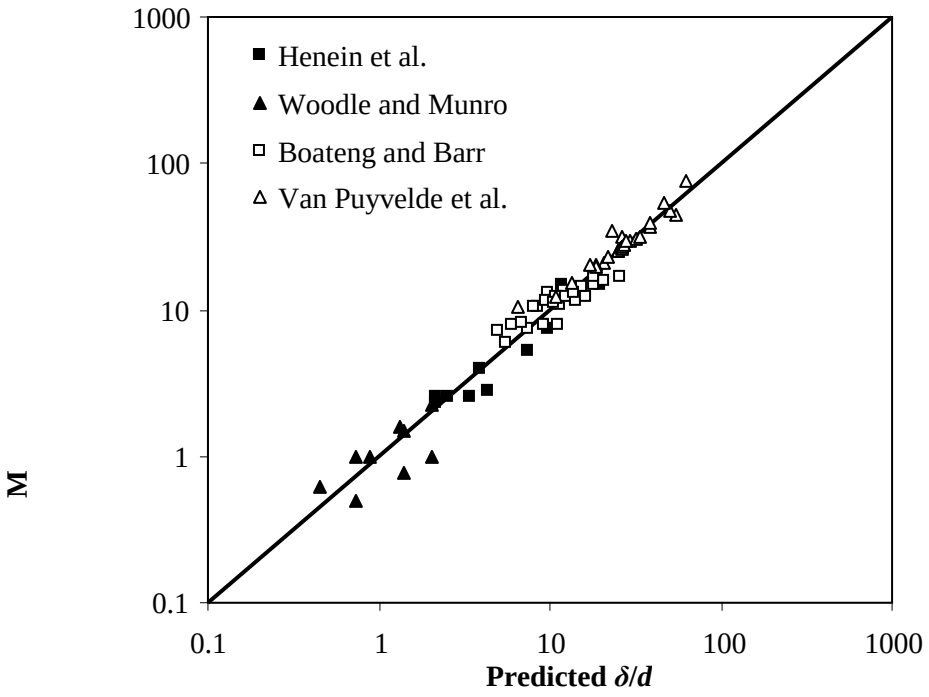


**Fig. 7.** Measured (Boateng and Barr [5], Henein et al. [11], Van Puyvelde et al. [12], and Woodle and Munro [13]) and predicted dimensionless maximum shear layer thickness. Solid line indicates perfect agreement.